Mechanical and corrosion properties of partially degradable bone screws

by A Kafrawi Nasution

Submission date: 17-Nov-2020 04:21PM (UTC+0800)
Submission ID: 1448799204
File name: de_of_pure_iron_and_stainless_steel_316L_by_friction_welding.pdf (7.87M)
Word count: 8843
Character count: 42410

SCIENCE CHINA Materials ARTICLES

mater.scichina.com link.springer.com

Published online 21 July 2017 | https://doi.org/10.1007/s40843-017-9057-3
Sci China Mater 2018, 61(4): 593–606

SPECIAL ISSUE: Advances in Metallic Biomaterials

Mechanical and corrosion properties of partially degradable bone screws made of pure iron and stainless steel 316L by friction welding

Ahmad Kafrawi Nasution[1], Mokhamad Fakhrul Ulum[2], Mohammed Rafiq Abdul Kadir[3] and Hendra Hermawan[4*]

ABSTRACT **This paper reports a series of *in vitro*, *ex vivo* and *in vivo* mechanical and corrosion studies of pin and screw prototype made of friction welded pure iron and 316L type stainless steel aiming to evaluate the applicability of the partially removable bone screws. Results showed that the pin possesses bending, tensile and torsional strengths of 1706±147, 666±7 and 0.34±0.03 MPa, respectively. The pin degraded at an average weight loss rate of 17.15×10^{-5} g cm^{-2} day^{-1} and released Fe ions at an average concentration of 2.38 ppm. Plastic deformation induced by torsion increased the corrosion rate of the pin from 0.0014 to 0.0137 mm year^{-1}. The maximum pull-out load of the screw prototypes was 3800 N with a calculated failure strength by shear load equal to 22.2 kN which is higher than the strength of the cortical bone. Detailed analysis of the rat's blood cells during 60 days of the pin implantation indicated a normal response with low neutrophils/lymphocytes ratio of 0.3–0.5. Iron ion concentration in the rat's blood slightly increased from 55 to 61 ppm without affecting the tissue recovering and healing phase. Histological evaluation confirmed the presence of macrophage cells as a normal response to the released iron particles around the iron section of the pin.**

Keywords: biodegradable metal, bone screw, friction welding, iron, stainless steel

INTRODUCTION

Metallic implants used for fixing fractured bone such as screws are usually removed after the fractured bone is healed and united. This procedure is normally done within a time span of one to two years to avoid bone refracture [1,2]. However, the necessity of this procedure is still debatable [3]. Although it is recommended to remove the screws when tissue rejection complications occur, e.g., an allergic reaction [3,4], the screws may still need to remain attached to the bones for functional reasons, e.g., avoiding bone refracture [5,6]. Beyond this debate, a partially removable bone screw is an interesting potential solution to address the controversy. The concept is that a half of the screw can be removed after the necessary healing period to avoid allergic reactions while the other half stays intact within the bone to avoid refracture. Thereafter, the intact part is expected to degrade progressively. At the end of the bone healing period, there will be no implant left behind while the bone returns to its normal biomechanical condition.

The above-mentioned concept needs a joint usage of inert materials such as type 316L stainless steel (SS316L) with biodegradable/bioabsorbable materials. Biodegradable orthopaedic implants have been in clinical use since a decade ago where biodegradable polymers such as the poly (lactic acid) and poly(caprolactone) families have been used as the materials [7]. However, creating a strong joint between metal and polymers for making a functional partially removable screw is not yet achievable by the current technological advances [8,9]. Fortunately, the emergence of new classes of biodegradable metals provides an ideal alternative. Three classes of metals have been

[1] Department of Mechanical Engineering, Faculty of Engineering, Muhammadiyah University of Riau, Pekanbaru 28122, Indonesia
[2] Faculty of Veterinary Medicine, Bogor Agricultural University, Bogor 16680, Indonesia
[3] Faculty of Biosciences and Medical Engineering, Universiti Teknologi Malaysia, Johor Bahru 81310, Malaysia
[4] Department of Mining, Metallurgical and Materials Engineering & CHU de Québec Research Center, Laval University, Quebec City G1V 0A6, Canada
* Corresponding author (email: hendra.hermawan@gmn.ulaval.ca)

increasingly studied as biodegradable metals: magnesium, iron and zinc and their alloys [7,10]. Their potential applications for orthopaedic implants have been extensively studied [11,12]. After the recent successful clinical trials [13,14], bone screws made of magnesium alloys are now commercially available for clinical use. In our previous work, we demonstrated that among the three classes of biodegradable metals, pure iron was successfully joined with SS316L by using a friction welding (FW) technique [15]. Thanks to the use of an optimum welding parameter, the welded metals possessed a good combination of strength and ductility and a gradual increase of corrosion rate from the stainless steel side to the pure iron side. It also showed no toxic effect on normal human osteoblast cells. In practical use of bone screws, the mechanical properties such as tensile, bending and torsional strengths are important qualities to ensure a successful installation and removal of the screws [16,17]. Their success also depends on other factors such as the screw diameter and design, the preparation of the hole and the bone mineral density [18,19]. In the case of a partially removable bone screw, considering the two welded dissimilar metals, special attention should be paid to the weld joint. Therefore, in the present work, we further studied the mechanical and corrosion properties of the pin and screw prototypes out of friction welded pure iron and SS316L. The pin and screw prototypes were subjected to various mechanical and corrosion tests. Also, *in vivo* study in rats was conducted to evaluate the suitability of the implants for orthopaedic applications.

EXPERIMENTAL SECTION

Friction welding and fabrication of screw prototype

Rods of annealed SS316L and drawn tempered pure iron (both with 9.5 mm diameter and 70 mm length, Goodfellow, UK) were used as base metals for FW and fabrication of the pin and bone screws. Chemical composition and mechanical properties of the rods are presented in Table 1. The surface of the rods has a roughness of 0.34±0.05 μm for SS316L and 0.62±0.06 μm for iron, measured by using a 3D digital microscope (Hirox KH-8700, Japan). By referring to our previous work [15], the FW was done on a modified lathe (Knuht DM 1000A –5.7 kW, Germany) using the following parameters: rotation spindle of 1600 rpm, forging pressure of 33.2 kPa, friction time of 25 s and long burn-off of 15 mm. All specimens were cut from the friction welded iron-SS316L rods with specific dimension according to the requirement for the various tests described in the following.

Following the design shown in Fig. 1, the bone screw prototypes were machined using a numerical controlled machine. All the processes and testing of bone screws were done according to the ASTM F543 standard and a product catalog of T-Bone Screws and Plates (Orthomed Inc., USA) [20]. Dimensional measurement of the screws was conducted by using Image-J NIH software (ImageJ* NIH, USA) and the results are presented in Table 2.

Mechanical and corrosion testing

Three modes of mechanical tests were performed: tensile, three-point bending and torsion. The tensile test was done in accordance with the ASTM E8 standard using a universal testing machine (Controlab-TN 20 MD, France) at a loading rate of 1.5 kN min^{-1}. Specimens for the tensile test (45 mm length, 6.0±0.1 mm diameter, 24.0±0.1 mm gauge length, and 6 mm fillet radius) were cut by a low speed precision sectioning machine (TechCut 5, Canada) and polished by an abrasive paper grit #800. The three-point bending test was done on rectangular specimens (2.8×5×16 mm^3) cut by an electrical discharge machine (Sodick AM3L EDM sinkers, USA). The three-point bending data were collected in accordance with the ASTM E290 standard using an axial-torsion fatigue testing system (Instron 8874, USA). The weld joint was loaded until the specimen bent into "U" shape. The bending strength was calculated using equation: $\sigma = 3PC/2wt^2$, where P is the force (N), C is the distance between lower supports (mm) ($C = 2r + 3t \pm t/2$), w is the specimen width and t is the specimen thickness (mm). Finally, the modulus of elasticity (E) was determined using equation: $E = mC^3/4wt^3$, where m is the slop of initial linear elastic portion of load-deection curve. The torsion test was done in accordance with the ASTM F1264 standard on specimens having dimension of 5 mm

Table 1 Chemical composition and mechanical properties of the base metals

Metal	Chemical composition (wt.%)									Mechanical properties		
	Fe	C	Mn	Si	P	S	Cr	Ni	Mo	UTS (MPa)	YS (MPa)	ε (%)
SS316L	Bal.	0.03	2.3	0.6	/	/	17.8	10.5	2.7	718	637	45
Iron	Bal.	0.002	0.009	0.003	/	/	/	/	/	702	582	9

UTS = ultimate tensile strength; YS = yield strength; and ε = maximum elongation.

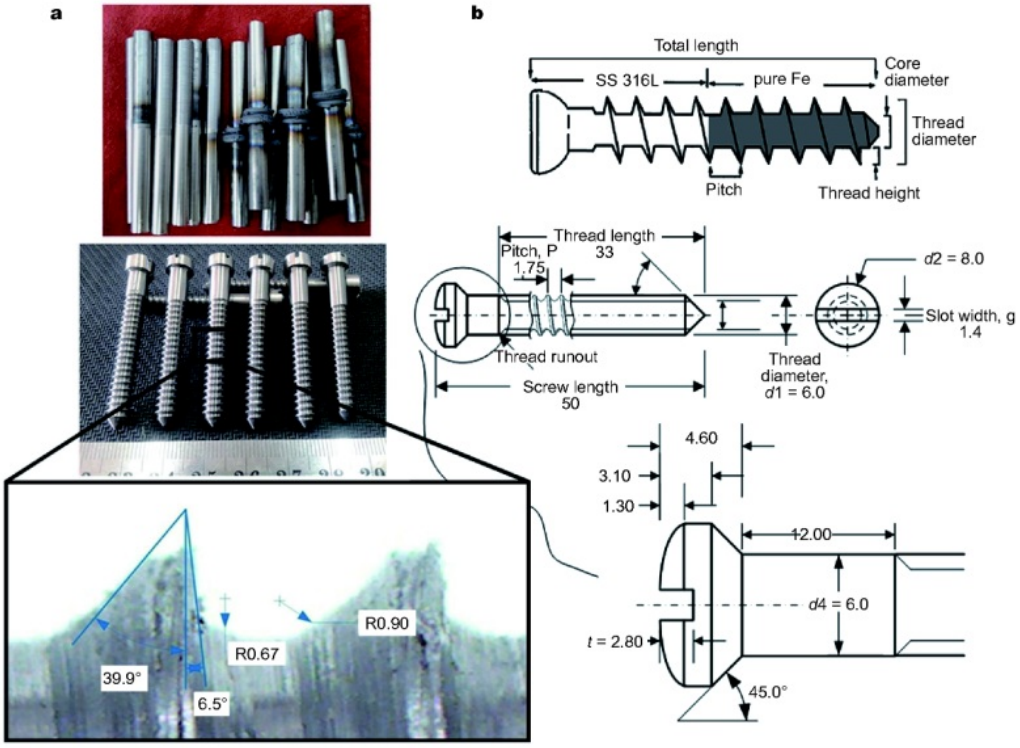

Figure 1 (a) Friction-welded rods and machined screw prototypes. (b) Schematic design of the cortical bone screws.

Table 2 Dimension of the bone screw prototype

Dimensional parameter	Value	Dimensional parameter	Value
Screw length (mm)	50	Slot width, g (mm)	1.4
Thread length (mm)	33	t (mm)	2.8
Thread diameter, $d1$ (mm)	6.0±0.6	Screw tip (°)	45
Head diameter, $d2$ (mm)	8.0	Leading edge radius, $r4$	0.9±0.1
Shaft diameter, $d4$ (mm)	6.0±0.6	Trailing edge radius, $r5$	0.5±0.1
Core diameter, $d5$ (mm)	4.7±0.6	Leading edge angle, α (°)	41.2±1.9
Thread pitch, P (mm)	1.75	Trailing edge angle, β (°)	7.4±2.3

diameter and 50 mm length using a manual machine due to limitation of the axial-torsion fatigue testing system in recognizing a torsional angle of less than 140°. Initially, the position of an unloaded specimen was fixed with a balancing water scale by placing an air bubble in the middle of the specimen. At this point, the torsion machine disc and the counter were classified as null. The disc was turned and the angle was recorded in relation with the corresponding force. This step was repeated with other angles and the resulting forces were recorded.

As shown in Fig. 2a, the pull-out test was performed using a section of a commonly fresh frozen two years old cow tibia, which was selected to mimic the mechanical strength of the human bone [21,22]. The cortical bone screw prototype was inserted manually with a screwdriver then extracted by a universal testing machine (Instron Fast Track 8874, USA) with displacement control at a fixed rate of 0.4 mm min^{-1}. The force was detected by a 25 kN load cell calibrated to be accurate within ±0.5% of the indicated force. The tests were repeated three times and all procedures were controlled under the provision of the ASTM F543 standard. Finally, the maximum tensile load (N) at a

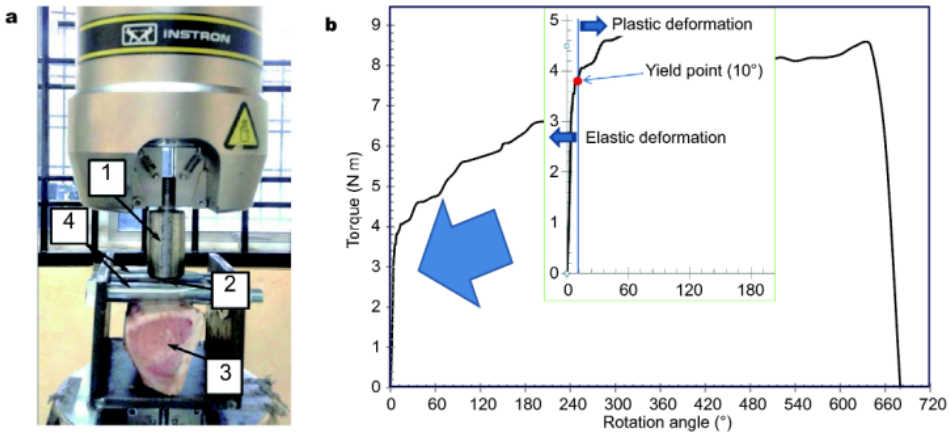

Figure 2 (a) Experimental set-up for uniaxial pull-out test. (b) Typical torsion test graph used for determining the elastic and plastic deformation limit. Note: (1) pull-out jig, (2) screw prototype, (3) grip span and (4) cow's tibia.

point when the screws were released from the cow bone was recorded to identify the pull-out strength.

Corrosion tests were carried out by two methods: simple immersion and immersion under torsion. Both methods used a simulated body uid (SBF) solution prepared based on the work of Kokubo and Takadama [23] with the following composition: 7.996 g NaCl, 0.350 g $NaHCO_3$, 0.224 g KCl, 0.228 g $K_2HPO_4{\cdot}3H_2O$, 0.305 g $MgCl_2{\cdot}6H_2O$, 40 cm^3 HCl (1 kmol m^{-3}), 0.278 g $CaCl_2$, 0.071 g Na_2SO_4, 6.057 g $NH_2C(CH_2OH)_3$. For the simple immersion, the specimens (3 mm diameter and 31 mm length) were immersed in 40 mL SBF at 37±1°C following the ASTM G31 standard for 1, 5, 25 and 60 days with five replications. The SBF solution was refreshed every 24 h and the weight loss of the specimens after cleaning was measured. The corrosion rate was calculated by using equation: $CR = m/St$ [24], where CR is the corrosion rate (g cm^{-2} day^{-1}), m is the weight loss (g), S is the surface area of the specimen, and t is the time (day). Changes in surface morphology were also observed under a stereo optical microscope (Motic Images Plus 2.0, China). Samples of 20 mL was collected from the immersion test solution and were subjected to ion concentration measurement using an atomic absorption spectrophotometer (AAS, AA-7000 Shimadzu, Japan). The corrosion products formed on the specimens after 60 days of immersion were analyzed using an X-ray diffractometer (XRD, Bruker D5000, Siemens, USA) at a scanning rate of 0.05° min^{-1} in the range between 20° and 90°. The immersion test under torsion was performed in 300 mL SBF at 37±1°C by means of a potentiostat (Versastat 3, Princeton Applied Research, USA) using a standard three-electrode conguration and a homemade torsional jig. Graphite served as the counter electrode, Ag/AgCl (KCl 3.5 mol L^{-1}) as the reference electrode and specimens under torsion (8.5 cm^2 exposed surface area) as the working electrode. The potentiodynamic polarization test was run at a scanning rate of 0.17 mV s^{-1} after a stable open-circuit potential was reached at 1800 s. The corrosion current (i_{corr}) and the corrosion potential (E_{corr}) were determined using Tafel extrapolation method and the corrosion rate was calculated using the equation: $CR = 3.27\times10^{-3} i_{corr} EW/\rho$, where EW is the equivalent weight and ρ is the density of the metal, in accordance with the ASTM G102 standard. The torsion load was adapted from the results of torsion test by setting the load limit of elastic and plastic deformations as shown in Fig. 2b.

In vivo study

The study was conducted after obtaining the ethical clearance from the Animal Ethics Committee, Bogor Agricultural University, Indonesia: 024/KEH/SKE/III/2015. Ten male rats (8 weeks, 180–190 g) were used as the animal model. Implant specimens (9×1.4×0.8 mm^3) were cut from the welded metals. The length of the implant includes three critical sections: iron section, iron-SS316L interface and SS316L section, as determined in our previous study [15]. The rats were subjected to a standard surgical procedure (acclimatization, implantation, monitoring, data collection and termination) under the supervision of the Animal Hospital of Bogor Agricultural University. They were given worm medicine (Praziquantel, 1 mg kg^{-1} weight) on day 1 and day 6, antibiotics

(Amoxicillin, 20 mg kg^{-1} weight) on day 2 to day 5, and anti-protozoa (Metronidazole, 20 mg kg^{-1} weight) until day 12 before the implantation phase. Environmental condition was controlled at 25–28°C with 60%–80% humidity. Before surgery, the rats were introduced with general anesthetic by injecting ketamine (50 mg kg^{-1} weight) and xylazine (5 mg kg^{-1} weight) into the intramuscular route. The implants were then implanted into the rat femurs with a defect of 10 mm length and 1.5 mm width, approximately (Fig. 3a). Five implants were implanted in each rat bone and fixed by suturing the surrounding muscles using an absorbable 5/0 Vicryl thread. The sutures were then closed with micropore patch. The rats were given antibiotics (Gentamicin, 1 mL/50 kg weight, 0.1 mL/rat tail) every two days for a total of five days. The control group was assigned for post-operative radiographic examination to visualize the correct placement of implants using a diagnostic X-ray unit (VR-1020 MA Medical, Japan). The rats were introduced to ketamine (50 mg kg^{-1} weight) and xilazin (5 mg kg^{-1} weight) before the imaging process for the anesthetic purpose. Further radiographs were taken as weekly follow-up (day 1, 7, 14, 30 and 60) to identify the morphological changes at the implantation site, such as bone formation. During the observation period, the rats underwent daily physical examination to specifically monitor the wound healing and the tissue growth at the implantation area.

Blood samples of 0.5 mL were withdrawn from the rat's tail vein before the implantation and on day 14, 30 and 60 post-implantation to monitor the systemic response. The concentrations of Fe and Ca ions in the blood plasma were determined using the AAS, while P ions by a UV spectrometer at 660 nm (LW Scientific, USA). For the purpose of retrieved implant observation, the rats were euthanized by injecting 25 mg sodium thiopental at 60 day post-implantation. A splitting cutting technique was used in lateral direction to remove the implant. The implant was then explanted and dried in a desiccator, while the femoral bone was also collected and dried in an oven at 40°C for two days (Fig. 3b) for further analyses by scanning electron microscopy-energy dispersive X-ray spectroscopy (SEM/EDS, TM3000 Hitachi, Japan). After exsanguination, the rat was then incised at implantation site to recover tissue samples (bone and muscle) for further pathological and histological evaluation. The remnant implant was explanted from the tissue, dried and stored in desiccated tube for further visual and chemical analysis. The tissue was fixed in buffered neutral 10% formaldehyde for further pathological anatomy observation using a stereo optical microscope (Motic Images Plus 2.0, China). The fixed tissue sample was decalcified in 5% nitric acid for 7 days, dehydrated stepwise through ascending series of alcohol solution and finally was degreased in xylene. The tissue was then embedded in paraffin block, sliced at 5 μm by microtome, and stained using hematoxylin and eosin (HE) stains. Cell response at the peri-implant tissue was observed under a CX31 optical microscope (Olympus, Japan) with digital image camera (XCAM1080PHA, China) to capture histological images at the metal interface.

RESULTS AND DISCUSSIONS

Table 3 shows the mechanical properties of the friction-welded specimens. Comparing these properties to those of the base metals (Table 1), it is observed that the tensile strength of the weld joint is 5%–7% lower than that of iron and SS316L. Also, its elongation is 70% lower and ~40% higher than that of the SS316L and the iron, respectively. Data from three-point bending test shows that the specimens achieved an ultimate strength of 1706±147 MPa, a yield strength of 656±96 MPa and a modulus of elasticity of ~18 GPa. The torsion test results show an ultimate torque of ~8 N m, an ultimate shear stress of 0.34±0.03

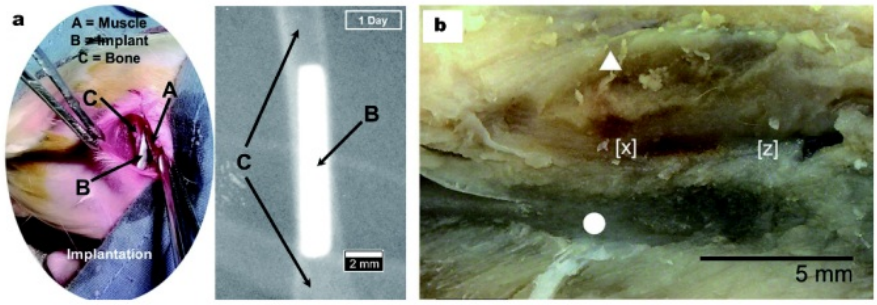

Figure 3 (a) Photograph and radiograph of implant placement in rat's femur, and (b) dried biopsy containing the implant in the right femur. Note: triangle = humeral muscle, circle = humerus bone, [x] iron side of the implant, [z] SS316L side of the implant.

Table 3 Mechanical properties of the friction-welded specimens

Tensile			Bending		Torsion		
σ_U (MPa)	σ_Y (MPa)	ε (%)	σ_U (MPa)	σ_Y (MPa)	M_T (N m)	τ_{max} (MPa)	G (GPa)
666±7	546±34	13±1	1706±147	656±96	8.3±0.8	0.34±0.03	0.26±0.02

Tensile: σ_U = ultimate tensile strength, σ_Y = yield strength, ε = maximum elongation; bending: σ_U = ultimate flexure stress, σ_Y = yield flexure stress; torsion: M_T = ultimate torque, τ_{max} = ultimate shear stress, G = modulus of rigidity.

MPa, a modulus of rigidity of 0.26±0.02 GPa and a maximum angle of rotation of ~630°.

In this work, a stable and non-oxidized weld joint was formed. The optimum combination of welding parameters, mainly friction time of 25 s and forging pressure of 16.6 kPa, and the smooth surface of the base metals were considered as the determined factor. Dey *et al.* [25] have shown that a fine surface of a workpiece resulted in a stronger weld joint. Meshram *et al.* [26] and Fukumoto *et al.* [27] stated that an optimum welding parameter, such as adequate heating and forging pressure, prevents the formation of oxide at the weld interface. The obtained torsional strength of the friction-welded specimens (Table 3) is higher than what is required in the ASTM F1264 standard for an intramedullary pin. The specimens with 3 and 5 mm diameter produced maximum torque of 3.27±0.31 and 8.3±0.78 N m, and breaking angle of 620±165° and 636±174°, respectively. However, in the ASTM F1264 standard, it is stated that pins with 3.5 and 5 mm diameter are supposed to produce a maximum torque of 2.3 and 5.5 N m, respectively, and a breaking angle of 180° for both the sizes. In this practical use (*in vivo* implantation of bone screw), the high torsion, tensile and bending strengths of the weld joint will ensure a successful installation and removal of the screw without failing due to fracture or bending.

Fig. 4 shows that a visible sign of corrosion appears on the weld joint and the iron section after 25 days of immersion in the SBF. A corrosion layer covered the whole specimen surface but started to peel off as the specimens were further immersed in the SBF till 60 days (Fig. 4d–e). The XRD analysis on the corrosion product of a 60 days immersed specimen (Fig. 4f) reveals several peak patterns identified as $Fe_3(PO_4)_2{\cdot}8H_2O$, $Fe(OH)_3$, $Mg_3(PO_4)_2$ and

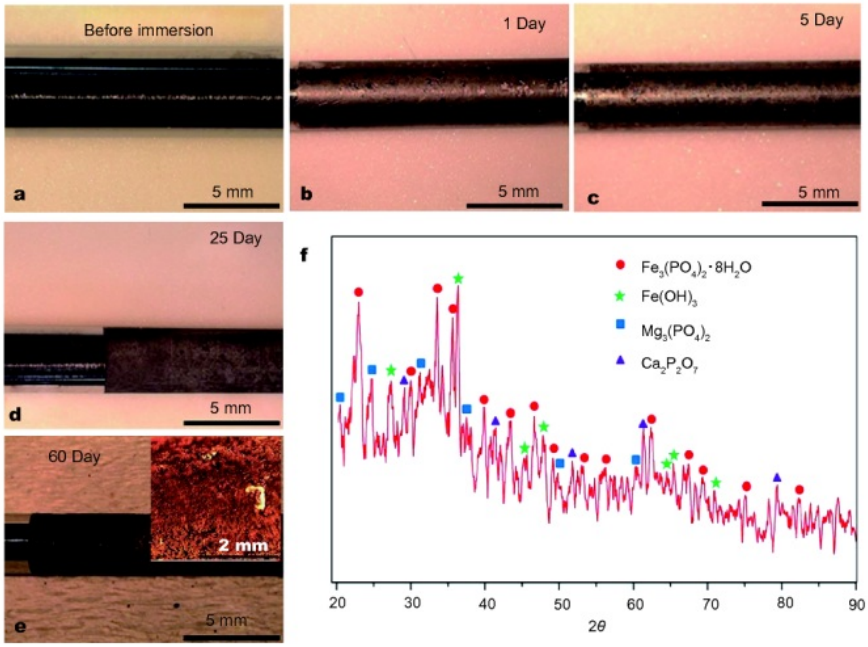

Figure 4 (a–e) Surface appearance of the corrosion specimens at different immersion times, and (f) XRD pattern of corrosion products on the 60 days immersed specimen.

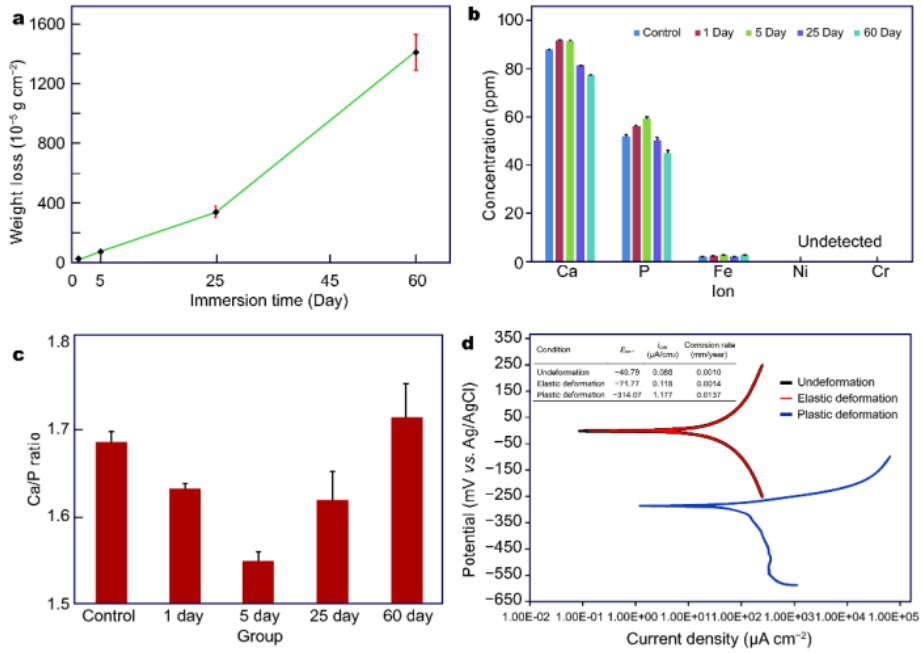

Figure 5 Corrosion behavior of the specimens plotted as: (a) weight loss, (b) concentration of ions released into the test solution, (c) Ca/P ratio of different groups, and (d) polarization curves of specimens under different torsion conditions.

$Ca_2P_2O_7$ compounds.

Fig. 5a shows the weight loss curve of the corrosion specimens over time. The weight loss curve is relatively linear with an indication of weight loss increase starting from 25 days to 60 days of immersion. This increase can be associated with the formation of iron hydroxide layer that formed but partially fell off around day 25. Similar result was observed on pure iron by Zhang *et al.* [28], where its corrosion rate slowly decreased from day 21 to day 28 of immersion. The average weight loss of the specimens in SBF solution is almost similar to the results obtained by Liu and Zheng [29] for pure iron in Hanks' solution which was 16.6×10^{-5} g cm^{-2}day^{-1}. This similarity confirms that SS36L section of the specimen did not involve in the corrosion process.

The ion concentration measurement (Fig. 5b) indicates the presence of Ca, P and Fe ions but the absence of Ni and Cr ions. The Ca and P elements come from the SBF solution. Due to some precipitation on the surface of the specimen, the Ca/P ratio decreases from day 1 to day 5, then it gradually increases until day 60 (Fig. 5c). The Ca/P ratio calculation may indicate the ability of the metal surface to form a hydroxyapatite-like layer that attracts bone cells [30]. In biodegradable implant applications, it is crucial to determine the amount of released Fe ions to ensure that it maintains the safety level in human body. Zhang *et al.* [28] proposed a theory that 25% of Fe ions released during 24 h immersion determines a safety level. The average weight loss of the specimen in 40 mL SBF solution was 17.15×10^{-5} g cm^{-2} day^{-1}, so the 25% of the 24 h immersion is 0.0429 mg mL^{-1}. Zhu *et al.* [31] reported that approximately a release of 0.05 mg mL^{-1} Fe ion is considered safe for the human body. Therefore, our results suggest that the concentration of Fe ions released from the specimen is within the safety level. The average concentration of 2.38 ppm Fe ion is equivalent to 0.0024 mg mL^{-1} which is still below the threshold reported by Zhu *et al.* [31]. The precipitation of Ca and P on the surface of the specimen is commonly observed, as the SBF solution is a rich source of these elements [32].

The results of electrochemical corrosion test on the specimens under torsion reveal that there was no noticeable difference in the corrosion potential (E_{corr}) between the deformed and the non-deformed specimens (Fig. 5d). The corrosion current density (i_{corr}) increased from 0.088 μA cm^{-2} for the non-deformed specimen to 0.118 μA cm^{-2} for the elastically deformed one with similar corrosion resistance value. The corrosion rates for the non-deformed

and the elastically deformed specimens are 0.0010 and 0.0014 mm year^{-1}, respectively. This indicates that elastic deformation by torsion did not affect corrosion behavior of the specimens. Meanwhile, the corrosion rate of the plastically deformed specimen is 0.0137 mm year^{-1}. This increase in corrosion rate was expected as a common phenomenon related to the stress concentration. Similar finding was reported by Harandi *et al.* [33] on deformed and cold worked magnesium alloys.

Fig. 6 shows that failure due to pull-out test of the screw occurred at the screw thread-cortical bone interface. The average pull-out force for the 4.7 mm screws was recorded at ~3800 N. Screw design such as thread diameter and pitch plays an important role in increasing the pull-out strength of the screw [34]. Wang *et al.* [35] stated that changing the screw geometry, especially adjusting the leading edge angle (α) to be less than 30°, increases the pull-out strength to 17%. However, increasing α up to 60° decreases the pull-out strength due to the reduction in "friction resistance" between the screw and the bone. A greater depth of thread and pitch leads to a higher pull-out strength of the screw which is due to greater holding capacity to the bones [36]. While the size of screw peak has no significant effect on the pullout strength [37], the screw length increases the pull-out strength due to higher contact or interface with the bone [38]. Therefore, the bone screw prototype in this work with a full length of 33 mm gives a high pull-out strength.

Additionally, the failure of screw after implantation becomes an important concern in design and manufacturing of bone screws. The calculated shear strength of the screw prototype in this work is 22.2 kN based on Chapman's equation [39]. This value is above the shear strength of the cortical bone suggested by Feerick and McGarry [40]. The maximum pull-out load of the screw prototype of about 3800 N is within the range of the pull-out load of a common cortical screw on composite femur of human cadaver (2600–7800 N) [41]. In the bone healing phase, the strength of bone screw is one of the important factors which supports the stiffness of the bone fixator beside the screw's core diameter and thread [42].

Fig. 7 shows the X-ray radiographic images at the im-

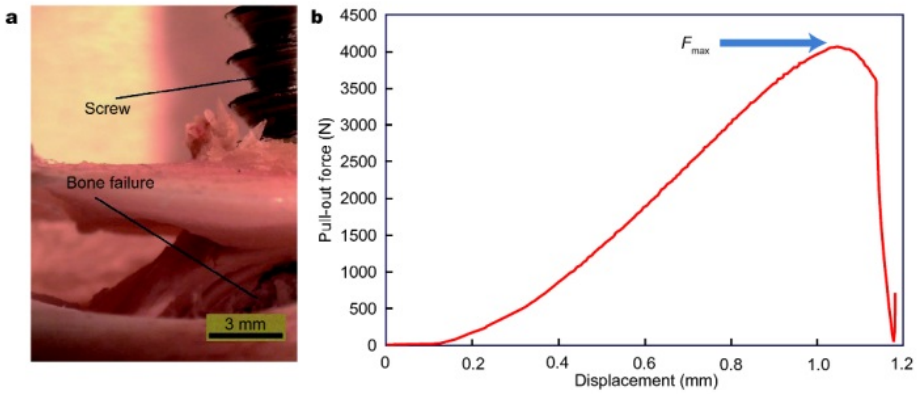

Figure 6 (a) An optical photograph of bone-screw configuration after pull-out test, and (b) a typical pull-out curve showing a load displacement experienced by the screw and the bone.

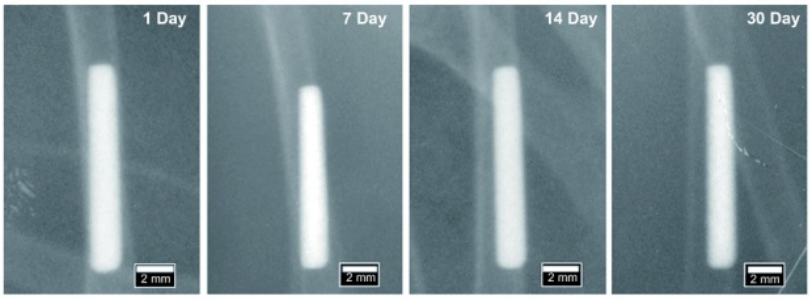

Figure 7 X-ray radiographic images of the implants at 1, 7, 14 and 30 days post-implantation.

plantation site indicating no visual evidence of bleeding, inflammation and gland formation (presence of exudates) around the implants at the 30 day post-implantation. This indicates a successful surgical procedure. Unlike iron-bioceramics implants that induce tissue formation [43], the iron-SS316L friction welded implant is considerably inert. Inflammation and tissue formation may not be detected by X-ray radiography, so they were investigated through the blood plasma analysis.

Table 4 presents a detailed blood cell analysis showing that red blood cell (RBC), hemoglobin (Hb), hematocrit (PCV), white blood cell (WBC) counts are all in a normal range at all time points. The lowest RBC count was observed on day 14 and the highest RBC count was observed on day 30. The Hb concentration ranges from 142 to 162 g L^{-1}, while the PCV count was recorded in between of 38.6% and 47.3%. The neutrophil/lymphocyte ratio changes from 0.3 on day 0 to 0.5 on day 60. The RBC, Hb and PCV counts are in the range of normal category indicating no visible response of toxicity. As part of the immune system, WBC helps the body to fight against various infections. The neutrophils, lymphocytes, eosinophils and monocytes counts are within the range of normal category, indicating no rejection reaction. The neutrophils/lymphocytes ratio of 0.3 to 0.5 is below the normal cellular stress response ratio of 1.5 [44].

Table 5 shows the concentrations of ions released into the blood plasma during the implantation period. The Cr and Ni ions were not detected. The Fe ion concentration decreases from 94 ppm on day 0 to 61 ppm on day 60, while the concentration of Ca ions slightly increases from 528 to 532 ppm from day 0 to day 60 post-implantation. An increment of Ca/P ratio is identified from 2.9 to 3.3. The Ca/P ratio of 3.3 for the iron-SS316L friction welded implant is close to that of inert SS316L implant (Ca/P ratio of 2.5) [30], which can indirectly confirm no inflammation has occurred. Inflammation usually leads to a reduction of Ca/P ratio due to imbalance of Ca and P minerals during inflammation [45]. Physiological reaction around the implant and its nearby tissues (muscle and bone) changes the ions concentration in blood plasma [46]. At 60 day post-implantation, Fe ion concentration on the implant

Table 4 Blood cell counts during the implantation period

Cell	Control group				Implant group				*p* value
	Day 0	Day 14	Day 30	Day 60	Day 0	Day 14	Day 30	Day 60	
RBC (10^6 cells μL^{-1})	8.2 ± 0.6^{ab}	8.5 ± 0.2^{ab}	8.8 ± 1.4^{ab}	7.1 ± 0.6^{a}	8.2 ± 0.6^{ab}	7.6 ± 0.8^{a}	10.8 ± 2.5^{b}	8.8 ± 1.2^{ab}	0.113
Hb (g dL^{-1})	14.2 ± 1.4^{ab}	15.4 ± 0.8^{c}	16.1 ± 1.2^{bc}	13.6 ± 0.3^{a}	14.2 ± 1.4^{ab}	15.2 ± 0.9^{abc}	16.2 ± 1.2^{bc}	14.3 ± 1.1^{ab}	0.053
PCV (%)	38.6 ± 1.2^{a}	42.8 ± 3.2^{cd}	40.3 ± 2.1^{ab}	42.6 ± 1.2^{bc}	38.6 ± 1.2^{a}	41.4 ± 1.2^{ab}	40.8 ± 1.6^{ab}	47.3 ± 2.8^{d}	0
WBC (10^3 cells μL^{-1})	9.7 ± 1.0^{b}	13.3 ± 2.6^{c}	9.1 ± 1.6^{b}	4.9 ± 1.9^{a}	9.7 ± 1.0^{b}	12.9 ± 1.2^{c}	13.5 ± 0.7^{c}	4.9 ± 1.2^{a}	0
Agranulocyte (%WBC)	77 ± 7.5^{a}	68.7 ± 11.6^{a}	65.7 ± 16.6^{a}	68.5 ± 9.2^{a}	77 ± 7.5^{a}	72.7 ± 7.6^{a}	70 ± 3.6^{a}	68 ± 1.7^{a}	0.755
Granulocyte (%WBC)	23 ± 7.5^{a}	31.3 ± 11.6^{a}	34.3 ± 16.6^{a}	31.5 ± 9.2^{a}	23 ± 7.5^{a}	27.3 ± 7.6^{a}	30 ± 3.6^{a}	32 ± 1.7^{a}	0.755
Lymphocyte (%WBC)	73.7 ± 7.8^{a}	65 ± 13.2^{a}	65.7 ± 16.6^{a}	66.5 ± 9.2^{a}	73.7 ± 7.8^{a}	70 ± 8.2^{a}	69.3 ± 4.2^{a}	66 ± 2.0^{a}	0.93
Monocyte (%WBC)	3.3 ± 1.2^{c}	3.7 ± 2.1^{bc}	0^{a}	2 ± 0.0^{bc}	3.3 ± 1.2^{c}	2.7 ± 1.5^{c}	0.7 ± 0.6^{ab}	2 ± 1.0^{bc}	0.008
Basophil (%WBC)	NIL^{a}	NIL^{a}	NIL^{a}	NIL^{a}	NIL^{a}	NIL^{a}	NIL^{a}	NIL^{a}	NIL
Neutrophil (%WBC)	22.7 ± 7.0^{a}	29.7 ± 11.2^{a}	34 ± 16.7^{a}	31 ± 8.5^{a}	22.7 ± 7.0^{a}	26 ± 7.9^{a}	30 ± 3.6^{a}	31.7 ± 1.5^{a}	0.701
Eosinophil (%WBC)	0.3 ± 0.6^{a}	1.7 ± 1.2^{b}	0.3 ± 0.6^{a}	0.5 ± 0.7^{a}	0.3 ± 0.6^{a}	1.3 ± 0.6^{ab}	0^{a}	0.3 ± 0.6^{a}	0.063
Neutrophil/lymphocyte	0.3 ± 0.1^{a}	0.5 ± 0.2^{a}	0.6 ± 0.4^{a}	0.5 ± 0.2^{a}	0.3 ± 0.1^{a}	0.4 ± 0.2^{a}	0.4 ± 0.1^{a}	0.5 ± 0.0^{a}	0.862

Data shown as mean with standard deviation (SD). The same letter in a different row indicates that the difference is not significant ($p > 0.05$).

Table 5 Concentrations of ions in rat's blood plasma

Ion	Concentration (ppm)			
	Control group		Implant group	
	Day 0	Day 60	Day 0	Day 60
Fe	94±1.5	55±4.1	94±1.5	61±2.3
Ca	528±8.2	528±3.4	528±8.2	532±6.4
P	181±1.4	169±4.1	181±1.4	161±3.4
Ca/P	2.9	3.1	2.9	3.3

group (61 ppm) is slightly higher compared to that of the control group (55 ppm) as a result of the corrosion process. The slight increase of Fe ion concentration could be the reason for the absence of excessive inflammation. This is desirable as in the period of 60 day post-implantation the tissue is still in the recovering and healing phase.

Fig. 8 shows the distribution of elements on the rat's muscle, the implant and the rat's bone at 60 day post-implantation. Both of the muscle regions (Fig. 8a) in contact with the iron section of the implant [x] and the SS316L section [z] are characterized by the presence of Fe, Ca and P at a similar percentage. On the implant surface (Fig. 8b), the content of P is higher than that on the muscle, while the content of Ca is lower. In the bone area (Fig. 8c), there is an increase of Ca content from ~23 wt.% at the iron section [x] to ~35 wt.% at weld joint section [y] and to ~40 wt.% at SS316L section [z]. A little amount of Ni was detected in [z]. The Ca/P ratio in bone areas of point [x], [y] and [z] is 2.5, 2.4 and 2.7, respectively. Fig. 8d–g show the elemental mapping taken on the cross-section of the retrieved rat's muscle and bone at 60 day post-implantation. The muscle region in contact with iron section of implant (Fig. 8d) shows an accumulation of Ca and P elements compared to the region in contact with SS316L section (Fig. 8e) where all elements are distributed evenly. The elemental mapping on the bone's cross-section shows a similar accumulation of Ca and P both at the region in contact with iron section (Fig. 8f) and with SS316L section (Fig. 8g). The implants were retrieved at 60 day post-implantation, a time during which the bone is not fully repaired and remodelled. A metal implant embedded in the body (*in vivo*) degrades due to electrochemical reaction between the metal and the body fluid [47]. The thickness of corrosion layer contributes to tissue swelling

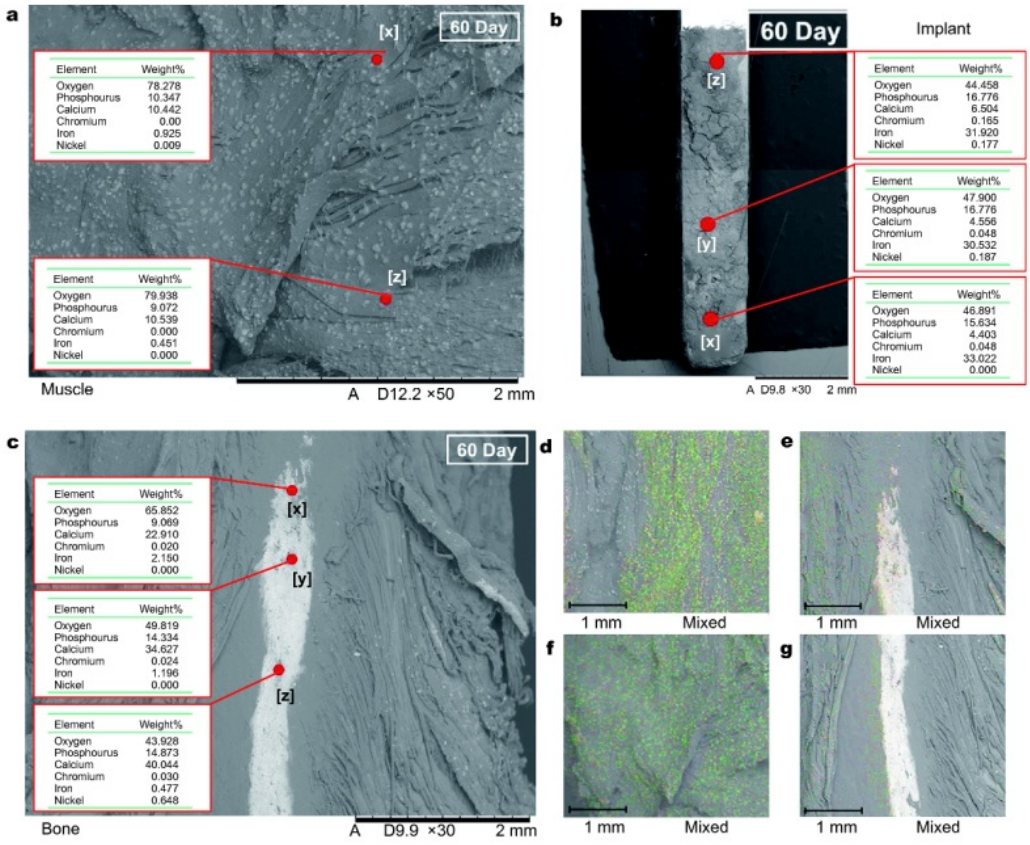

Figure 8 SEM/EDS observation on: (a) the rat's muscle, (b) implant, (c) rat's bone, (d, e) elemental mapping on the cross-section of rat's muscle around [x] and [z], and (f, g) elemental mapping on the cross-section of rat's bone around [x] and [z], all at 60 day post-implantation. Note: [x] pure iron section, [y] weld joint section, and [z] SS316L section.

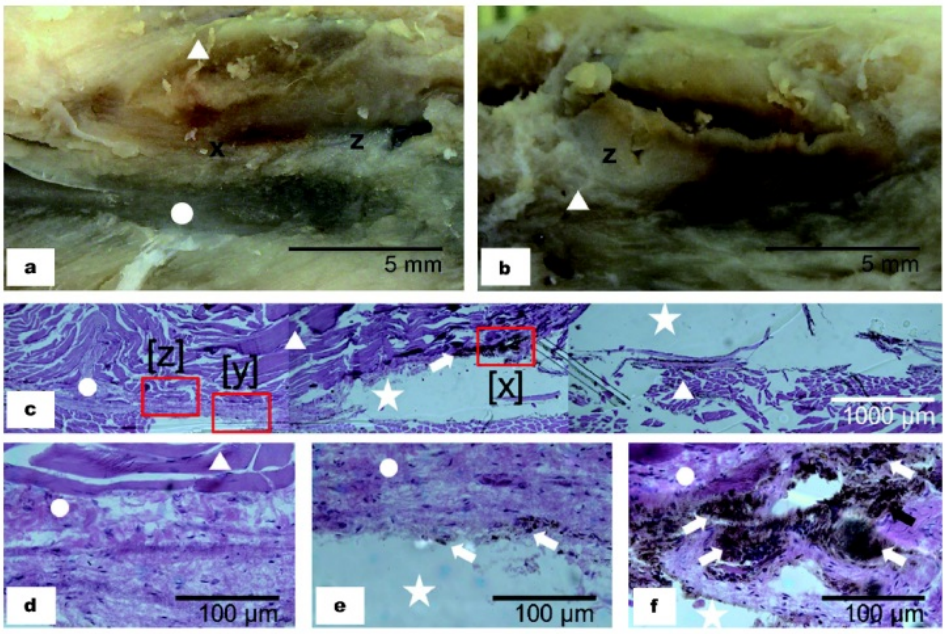

Figure 9 Pathological images of tissue around implant taken at 60 day post-implantation showing (a) sagittal and (b) lateral view. (c) Histological images at low magnification, and (d, e, f) high magnification of region in contact with SS316L section [z], weld joint section [y] and iron section [x], respectively. Note: triangle = humeral muscle, circle = humerus bone, star = void (implant region), white arrow = corrosion product, black arrow = macrophages.

during the wound healing [48]. As shown in Fig. 8d-g, a thin corrosion layer is present on the surface of the implant at 60 day post-implantation with small distribution of Fe in the local muscle tissue as well as in the bone tissue.

Fig. 9a, b depict a pathological anatomy of a fixed implantation tissue. It can be seen that the iron section of the implant released corrosion products into the peri-implant tissue marked by the brown color. This is not seen on the tissue in contact with the SS316L section. Fig. 9c-f show the histological images of peri-implant tissue at 60 day post-implantation. Corrosion product particles are observed in the surrounding implantation site with a higher accumulation on the region where there was a contact with the iron section of the implant. A higher number of macrophage cells are also observed at the accumulation site indicating a higher cellular response to the corrosion products. Neither corrosion products nor macrophage cells are found in the region which was previously in contact with SS316L section.

The microscopic finding in histological evaluation portrays the accumulation of brown corrosion product particles within the peri-implant site. This has similarity with the result reported in the study of Paramitha *et al.* [49] where the brown particles from iron-based implants were distributed within the surrounding tissue of implantation site. Ulum *et al.* [30] reported that a high cellular activity occurred at peri-implant of iron-bioceramic composite implants. These particles have been the object for macrophage cells to digest as indicated by the significant higher monocyte cell count in the implant group compared to the control group (Table 4). Monocyte cells from the bloodstream transform into macrophages and go into the surrounding implantation site where the corrosion product particles are present [30]. Even though the radiological image analysis is not capable to distinguish the corrosion products, the decreasing radiodensity of the iron section of implant (Fig. 7) is proportional with the pathological anatomy and the histological patterns (Fig. 9). The observed decrease of radiodensity shows a similarity with the radiodensity analysis of iron-bioceramics implants at 70 day post-implantation [43].

CONCLUSIONS

This work demonstrated a successful friction welding technique in joining pure iron and type 316L stainless steel as well as prototyping of partially degradable bone screws. As a result of choosing an optimum welding parameter, the measured values of bending, tensile and torsional

strengths were higher than those are suggested in the ASTM F543 standard. Corrosion occurred only on the iron side of the friction welded specimen with an increase on the weight loss rate from day 25 to day 60 of immersion. Nickel or chromium ions were undetected in the corrosion test solution whilst the concentration of iron ions was below the safe threshold value. The corrosion rate of the specimens increased by 10 folds due to plastic deformation induced by torsion. The bone screw prototypes possess a high pull-out strength of 3800 N which is within the range of the pull-out load of a comparable cortical screw on composite femur human cadaver. The detailed blood cell counts during implantation of the implants in rats indicated a normal body response without excessive inflammatory reaction. The slight increase of iron ion concentration in rat's blood did not affect the tissue recovering and healing phase. After 60 days of implantation, a thin corrosion layer was formed on the implant surface and elemental Fe was found in the local muscle tissue and in the bone. Histological evaluation on the area of contact with the implant showed a normal presence of macrophage cells at the iron section but an absence of them at the stainless steel section. This work suggests that there is a potential applicability of partially removable bone screw concept made of iron and stainless steel joined by friction welding.

Received 17 April 2017; accepted 25 May 2017; published online 21 July 2017

1 Hidaka S, Gustilo RB. Refracture of bones of the forearm after plate removal. J Bone Joint Surg, 1984, 66: 1241–1243
2 Bostman O, Pihlajamaki H. Routine implant removal after fracture surgery. J Trauma-Injury Infection Critical Care, 1996, 41: 846–849
3 Vos DI, Verhofstad MHJ. Indications for implant removal after fracture healing: a review of the literature. Eur J Trauma Emerg Surg, 2013, 39: 327–337
4 Hallab N, Merritt K, Jacobs JJ. Metal sensitivity in patients with orthopaedic implants. J Bone Joint Surg Am, 2001, 83: 428–436
5 Brown OL, Dirschl DR, Obremskey WT. Incidence of hardware-related pain and its effect on functional outcomes after open reduction and internal fixation of ankle fractures. J Orthopaedic Trauma, 2001, 15: 271–274
6 Busam ML, Esther RJ, Obremskey WT. Hardware removal: indications and expectations. J Am Acad Orthopaedic Surg, 2006, 14: 113–120
7 Nasution AK, Hermawan H. Degradable biomaterials for temporary medical implants. Adv Struct Mater, 2016, 58: 127–160
8 Kah P, Suoranta R, Martikainen J, et al. Techniques for joining dissimilar materials: metals and polymers. Rev Adv Mater Sci, 2014, 36: 152–164
9 Amancio-Filho ST, dos Santos JF. Joining of polymers and polymer-metal hybrid structures: recent developments and trends. Polym Eng Sci, 2009, 49: 1461–1476
10 Zheng YF, Gu XN, Witte F. Biodegradable metals. Mater Sci Eng-R-Rep, 2014, 77: 1–34
11 Staiger MP, Pietak AM, Huadmai J, *et al.* Magnesium and its alloys as orthopedic biomaterials: a review. Biomaterials, 2006, 27: 1728–1734
12 Hort N, Huang Y, Fechner D, *et al.* Magnesium alloys as implant materials-principles of property design for Mg-RE alloys. Acta Biomater, 2010, 6: 1714–1725
13 Windhagen H, Radtke K, Weizbauer A, *et al.* Biodegradable magnesium-based screw clinically equivalent to titanium screw in hallux valgus surgery: short term results of the first prospective, randomized, controlled clinical pilot study. BioMed Eng OnLine, 2013, 12: 62
14 Lee JW, Han HS, Han KJ, *et al.* Long-term clinical study and multiscale analysis of *in vivo* biodegradation mechanism of Mg alloy. Proc Natl Acad Sci USA, 2016, 113: 716–721
15 Nasution AK, Murni NS, Sing NB, *et al.* Partially degradable friction-welded pure iron-stainless steel 316L bone pin. J Biomed Mater Res, 2015, 103: 31–38
16 Ivanoff CJ, Sennerby L, Johansson C, *et al.* Influence of implant diameters on the integration of screw implants. Int J Oral Maxillofac Surgery, 1997, 26: 141–148
17 Klokkevold PR, Johnson P, Dadgostari S, *et al.* Early endosseous integration enhanced by dual acid etching of titanium: a torque removal study in the rabbit. Clin Oral Implants Res, 2001, 12: 350–357
18 Yerby S, Scott CC, Evans NJ, *et al.* Effect of cutting flute design on cortical bone screw insertion torque and pullout strength. J Orthopaedic Trauma, 2001, 15: 216–221
19 Wilmes B, Drescher D. Impact of bone quality, implant type, and implantation site preparation on insertion torques of mini-implants used for orthodontic anchorage. Int J Oral Maxillofac Surg, 2011, 40: 697–703
20 OrthoMed. Surgical Instruments Product Catalog. 2013
21 Taylor D. Scaling effects in the fatigue strength of bones from different animals. J Theor Biol, 2000, 206: 299–306
22 Topp T, Müller T, Huss S, *et al.* Embalmed and fresh frozen human bones in orthopedic cadaveric studies: which bone is authentic and feasible? Acta Orthopaedica, 2012, 83: 543–547
23 Kokubo T, Takadama H. How useful is SBF in predicting *in vivo* bone bioactivity? Biomaterials, 2006, 27: 2907–2915
24 Huang T, Cheng J, Zheng YF. *In vitro* degradation and biocompatibility of Fe-Pd and Fe-Pt composites fabricated by spark plasma sintering. Mater Sci Eng-C, 2014, 35: 43–53
25 Dey HC, Ashfaq M, Bhaduri AK, *et al.* Joining of titanium to 304L stainless steel by friction welding. J Mater Proc Tech, 2009, 209: 5862–5870
26 Meshram SD, Mohandas T, Reddy GM. Friction welding of dissimilar pure metals. J Mater Proc Tech, 2007, 184: 330–337
27 Fukumoto S, Katayama K, Okita K, *et al.* Small-scale friction welding of similar and dissimilar stainless steels. Quart J Japan Weld Soc, 2009, 27: 99s–103s
28 Zhang E, Chen H, Shen F. Biocorrosion properties and blood and cell compatibility of pure iron as a biodegradable biomaterial. J Mater Sci-Mater Med, 2010, 21: 2151–2163
29 Liu B, Zheng YF. Effects of alloying elements (Mn, Co, Al, W, Sn, B, C and S) on biodegradability and *in vitro* biocompatibility of pure iron. Acta Biomater, 2011, 7: 1407–1420
30 Ulum MF, Nasution AK, Yusop AH, *et al.* Evidences of *in vivo* bioactivity of Fe-bioceramic composites for temporary bone implants. J Biomed Mater Res, 2015, 103: 1354–1365

31 Zhu S, Huang N, Xu L, *et al*. Biocompatibility of pure iron: *in vitro* assessment of degradation kinetics and cytotoxicity on endothelial cells. Mater Sci Eng-C, 2009, 29: 1589–1592
32 Witte F, Kaese V, Haferkamp H, *et al*. *In vivo* corrosion of four magnesium alloys and the associated bone response. Biomaterials, 2005, 26: 3557–3563
33 Harandi SE, Hasbullah Idris M, Jafari H. Effect of forging process on microstructure, mechanical and corrosion properties of biodegradable Mg–1Ca alloy. Mater Des, 2011, 32: 2596–2603
34 Krenn MH, Piotrowski WP, Penzkofer R, *et al*. Influence of thread design on pedicle screw fixation. J Neurosurgery-Spine, 2008, 9: 90–95
35 Wang Y, Mori R, Ozoe N, *et al*. Proximal half angle of the screw thread is a critical design variable affecting the pull-out strength of cancellous bone screws. Clin Biomech, 2009, 24: 781–785
36 Ferrara LA, Ryken TC. Screw pullout testing. In An YH, Draughn RA (Eds.). Mechanical Testing of Bone and the Bone-implant Interface. Boca raton-Florida: CRC Press, 2000
37 Mehta H, Santos E, Ledonio C, *et al*. Biomechanical analysis of pedicle screw thread differential design in an osteoporotic cadaver model. Clin Biomech, 2012, 27: 234–240
38 DeCoster TA, Heetderks DB, Downey DJ, *et al*. Optimizing bone screw pullout force. J Orthopaedic Trauma, 1990, 4: 169–174
39 Patel PSD, Shepherd DET, Hukins DWL. The effect of screw insertion angle and thread type on the pullout strength of bone screws in normal and osteoporotic cancellous bone models. Med Eng Phys, 2010, 32: 822–828
40 Feerick EM, McGarry JP. Cortical bone failure mechanisms during screw pullout. J Biomechanics, 2012, 45: 1666–1672
41 Zdero R, Rose S, Schemitsch EH, *et al*. Cortical screw pullout strength and effective shear stress in synthetic third generation composite femurs. J Biomech Eng, 2007, 129: 289–293
42 Asnis SE, Ernberg JJ, Bostrom MPG, *et al*. Cancellous bone screw thread design and holding power. J Orthopaedic Trauma, 1996, 10: 462–469
43 Ulum MF, Arafat A, Noviana D, *et al*. *In vitro* and *in vivo* degradation evaluation of novel iron-bioceramic composites for bone implant applications. Mater Sci Eng-C, 2014, 36: 336–344
44 Kannan G, Terrill TH, Kouakou B, *et al*. Transportation of goats: effects on physiological stress responses and live weight loss. J Animal Sci, 2000, 78: 1450–1457
45 Conz MB, Granjeiro JM, Soares GA. Hydroxyapatite crystallinity does not affect the repair of critical size bone defects. J Appl Oral Sci, 2011, 19: 337–342
46 Langton DJ, Sidaginamale RP, Joyce TJ, *et al*. The clinical implications of elevated blood metal ion concentrations in asymptomatic patients with MoM hip resurfacings: a cohort study. BMJ Open, 2013, 3: e001541
47 Schmutz P, Quach-Vu N-C, Gerber I. Metallic medical implants: electrochemical characterization of corrosion processes. Electrochem Soc Interf, 2008, 17: 35–40
48 Carrodeguas RG, De Aza S. α-Tricalcium phosphate: synthesis, properties and biomedical applications. Acta Biomater, 2011, 7: 3536–3546
49 Paramitha D, Estuningsih S, Noviana D, *et al*. Distribution of Fe-based degradable materials in mice skeletal muscle. Eur Cell Mater, 2013, S5: 55

Acknowledgements This work was supported by the Malaysian Ministry of Higher Education, the Indonesian Ministry of Education and Culture and the Natural Sciences and Engineering Research Council of Canada (NSERC). The authors thank Panjaitan B, Paramitha D, Setiadi MA and Karja NWK for their help during the *in vivo* animal implantation and histological analysis.

Author contributions All authors contributed to the preparation and discussion of the manuscript. The final version of the manuscript was approved by all authors.

Conflict of interest The authors declare that they have no conflict of interest.

Ahmad Kafrawi Nasution received his PhD degree in biomedical engineering from the University of Technology of Malaysia in 2016 under the supervision of Dr. Hermawan and Dr. Abdul Kadir. He is now a lecturer at the Department of Mechanical Engineering, Muhammadiyah University of Riau in Indonesia where he is building a research group on biomaterials.

Mokhamad Fakhrul Ulum received his PhD degree in biomedical engineering from the University of Technology of Malaysia in 2016 under the supervision of Dr. Hermawan and Dr. Abdul Kadir. He is now a lecturer at the Faculty of Veterinary Medicine, Bogor Agricultural University in Indonesia where he was previously trained as veterinarian.

Mohammed Rafiq Abdul Kadir received his PhD degree in medical engineering from Imperial College London in 2005. He is now a professor at the Faculty of Biosciences and Medical Engineering, University of Technology of Malaysia in Malaysia leading an active research center in medical devices technology (MediTeg).

Hendra Hermawan received his PhD degree in materials engineering from Laval University in 2009. After spending some academic years in Asia, he returned to Laval University in 2014 as an assistant professor and also researcher at CHU de Québec Research Center, Québec, Canada. His research interests include biomaterials, biodegradable metals and corrosion.

Mechanical and corrosion properties of partially degradable bone screws

ORIGINALITY REPORT

18%	7%	10%	3%
SIMILARITY INDEX	INTERNET SOURCES	PUBLICATIONS	STUDENT PAPERS

MATCH ALL SOURCES (ONLY SELECTED SOURCE PRINTED)

4%

★ Mokhamad F. Ulum, Ahmad K. Nasution, Abdul H. Yusop, Andril Arafat et al. " Evidences of bioactivity of Fe-bioceramic composites for temporary bone implants ", Journal of Biomedical Materials Research Part B: Applied Biomaterials, 2015

Publication

Exclude quotes	On	Exclude matches	< 3%
Exclude bibliography	On		